FACULTY OF PHYSICS AND ASTRONOMY
UTRECHT UNIVERSITY

Bachelor thesis
in Physics

submitted by
Oliver K. Ernst

June 20, 2013

Hard Probe Observables of Jet Quenching in the Monte Carlo Event Generator JEWEL

This Bachelor thesis has been carried out by Oliver K. Ernst at the
Institute for Subatomic Physics
under the supervision of
Marco van Leeuwen and Misha Veldhoen

Abstract

The jet quenching effects of including recoil partons from interactions of high momentum partons with the QGP in Pb+Pb events are studied in the JEWEL Monte Carlo Event Generator. Momentum balance in the model shows that excluding recoil partons leads to a net momentum imbalance on the order of tens of GeV/c, indicating the necessity to include recoil partons in observables that depend on momentum conservation. When calculating the nuclear modification factor R_{AA}, the generation of recoil hadrons that result from the hadronization of recoil partons requires a background subtraction procedure to be implemented due to the high number of recoil tracks as compared to benchmark p+p events. Furthermore, the non-uniform distribution of recoil tracks in pseudorapidity presents both a conceptual curiosity and exceptional challenges in sampling the recoil track background, in particular, choosing the region in the ϕ, η plane to sample for the density of jet transverse momentum. Several regions are compared for cone radii used in jet finding ranging from $R = 0.2$ to $R = 0.5$. We find that including recoil partons leads to a dependence of the nuclear modification factor on the cone radius that is not observed when recoil partons are excluded.

Contents

1 Introduction

One of the frontier research topics in high energy physics is the study of the theory of the strong interaction, QCD (Quantum Chromo Dynamics). The fundamental constituents of QCD matter are quarks and gluons, which are confined in nature to exist only as color neutral combinations in the form of baryons and mesons. However, at high energy densities, a deconfined state of matter is predicted to exist, in which quarks and gluons are deconfined in a QGP (Quark Gluon Plasma).

Great experimental and theoretical effort has been dedicated to the production and study of the QGP. At the ALICE (A Large Ion Collider Experiment) experiment at the LHC (Large Hadron Collider), collisions of Pb nuclei at $\sqrt{s} \approx 2.76\,\mathrm{TeV}/c$ are expected to produce this deconfined medium [1]. Still, a number of nontrivial obstacles complicate its direct study. In particular, the rapid expansion and cooling of the medium leads to a short lifetime on the order of several fm/c_0. Hence, there exist only a limited number of probes of the QGP.

The study of partons produced in the collision with large transverse momentum $p_T \gtrsim 1\,\mathrm{GeV}/c$ is of particular interest, since they can be theoretically described using pQCD (pertubative QCD) [2]. Since these partons are produced on time-scales $\tau \approx 0.1\,\mathrm{fm}/c_0$ [2], they are expected to propagate through and interact with the medium before it cools, producing showers of partons. These showers consequently hadronize to form jets. Measurements of both the dijet asymmetry and the high momentum jet suppression in these collisions indicate that the high momentum partons will dissipate a significant fraction of their energy at large angles to the medium. This “jet quenching" is one of the key signatures of (the) QGPs formation, and can be used to study the properties of this matter.

Monte Carlo (MC) event generators provide a powerful technique to simulate nucleus-nucleus collisions. In this thesis, we study the observables of jet quenching in the MC event generator JEWEL (Jet Evolution With Energy Loss), described in detail in [3] [4].

The measurement of the suppression of high momentum jets in particular raises several questions regarding the method by which the collision is modeled in JEWEL, and furthermore the procedure by which jets of hadrons are reconstructed in the event. We also examine momentum balance in the MC, and qualitatively compare these results to CMS data.

Much of this work is dedicated to the study of hadrons that stem from interactions between the hard probe and the medium, but that are not included by default in the final output of JEWEL. We explore the validity of a background subtraction procedure that allows us to include these hadrons in hard probe observables, and examine how they influence the observed jet quenching.

2 Jet Quenching

2.1 Jets and Jet Quenching

Jets are the result of the fragmentation and subsequent hadronization of a high momentum parton into a spray of partons with momenta at small angles with respect to each other [2]. In Pb+Pb collisions, when a hard scattering process occurs, the resulting partons are produced back-to-back in the transverse plane due to momentum conservation. Since these processes can occur anywhere in plasma, both partons consequently have to traverse and interact with the medium. However, while in some cases one parton may traverse only a small region of the medium before going into the vacuum, the other suffers energy loss from gluonstrahlung in the dense plasma before fragmenting into a jet [2]. Hence, the former parton will form a high momentum jet, while the other will radiate a fraction of its original energy to produce low momentum particles at large azimuthal angles relative to the largest transverse momentum (leading) jet axis. This quenching effect leads to a suppression of jets produced at high transverse momentum in comparison to benchmark pp collisions, where no QGP is produced.

One way to quantify this suppression is through the nuclear modification factor R_{AA}, the ratio of the yield of the collision of two nuclei A compared to the yield in p+p collisions, defined as

$$R_{\mathrm{AA}} = \frac{1}{N_{\mathrm{evt}}} \left(\frac{d^2 N^{\mathrm{AA}}}{dp_{\mathrm{T}} d\eta} \right) \left(\langle T_{\mathrm{AA}} \rangle \frac{d^2 \sigma^{\mathrm{pp}}}{dp_{\mathrm{T}} d\eta} \right)^{-1}. \tag{2.1}$$

Here T_{AA} is the nuclear overlap function, defined as the ratio of the number of binary nucleon-nucleon collisions $\langle N_{\mathrm{coll}} \rangle$ calculated from a Glauber model of the the nuclear collision geometry [5] and the inelastic nucleon-nucleon cross section $\sigma_{\mathrm{inel}}^{\mathrm{NN}} = (64 \pm 5)\mathrm{mb}$ at $\sqrt{s} = 2.76\,\mathrm{TeV}/c$ [6].

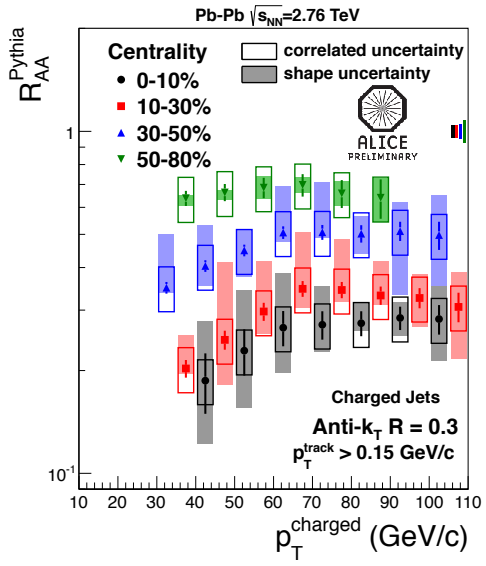

Figure 2.1: Jet R_{AA} for various centrality bins from the ALICE collaboration. Taken from [7].

The nuclear modification factor is largely dependent on both p_{T} and $\sqrt{s}$. To study in particular the p_{T} dependence, we observe both spectra of charged hadron p_{T} produced in the event, and reconstructed jet p_{T}. A nuclear modification factor below unity is indicative of jet quenching, with data from both experiment and JEWEL as presented in [3] showing an approximate suppression of $R_{\mathrm{AA}} \approx 0.2$.

From experimental data as presented in [7] as shown in Figure 2.1, the nuclear modification factor is slightly positively correlated with jet p_{T}. The same effect is observed in spectra of charged hadron R_{AA}. In fact, for charged hadrons the factor may continue to rise above unity at high p_{T}, as observed in [3]. A tentative

explanation is that at very large p_T, the effect of energy loss starts to diminish. It is postulated in [3] that this is due to a kinematical effect where very high energetic partons convert longitudinal into transverse momentum in elastic scatterings. This effect is largely dependent on the medium model employed, particularly on the density of scattering centers in the medium. Hence, the trend presents a testable prediction that can be used for the validation of JEWEL [3].

A further method of quantifying the extent of jet quenching is through the asymmetry in the transverse momentum between the two leading momentum jets produced by the hard scattering. From previous work such as [3] [4], it is postulated that jet quenching causes much of the energy of the quenched subleading jet to be radiated at large angles to the leading jet axis. Thus, highly quenched events in Pb+Pb events will have large difference between the leading and subleading jet p_T, while p+p baseline events will have a lower difference.

2.2 Jet Finding

Analogous to the data collected in experimental collisions at the LHC, jets in JEWEL events are not tracked in their production from the original hard partons, and hence must be reconstructed from showers of hadrons. For our analysis, we use the FastJet v3.0.4 C++ package to perform jet finding [8]. Several well known algorithms exist to perform jet finding, and the results presented in this thesis are largely dependent on the jet finding routine performed. For consistency, the *anti-kt* algorithm was used throughout this analysis, as described in detail in [9].

The algorithm uses a cone radius parameter, $R \equiv \sqrt{(\Delta\eta)^2 + (\Delta\phi)^2}$, to determine which tracks in the η, ϕ plane to include in a single jet. A significant focus of the present work is studying the effect of varying the cone radius on R_{AA}. Unless otherwise indicated, all charged tracks with $p_T^{track} > 0.15\,\mathrm{GeV}/c$ are included in the jet finding, following [7]. Since the transverse momentum of a jet corresponds to the sum transverse momenta of its constituent tracks, then increasing the cone radius is expected to yield fewer jets, each with higher p_T. Hence, the yield of jets as a function of jet p_T and thus the jet R_{AA} is expected to be dependent on the cone radius used.

3 JEWEL

3.1 Motivation for the model

Collisions with high momentum transfer occur in a regime that is calculable using pQCD, and so can be simulated with MC event generators. Several MC models have been developed that incorporate various energy loss models to simulate jet quenching - in particular, HIJING [10] and Q-PYTHIA [11].

The JEWEL event generator is described in detail in [3] [4]. It has the advantage over previous MC models in that it uses both collisional and radiative parton energy loss mechanisms to model the effects of jet quenching. Furthermore, pQCD matrix elements are continued into the infra-red region, and so the dominant effect of soft scatterings can be included. However, this also leads to great uncertainties in the non-pertubative regime, and extent to which soft interactions can be accurately described is ambiguous.

3.2 Implementation Overview

JEWEL events are based on medium modifications to parton showers produced by the event generator PYTHIA 6.4 [12]. The procedure by which events are generated is summarized as follows:

1. Initial parton showers are generated from hard scatterings in PYTHIA.
2. The showers are passed to JEWEL, which calculates the energy loss from interactions with the medium. JEWEL models the medium as a collection of partons with a fixed distribution is phase space. In interactions of the jet with the medium, the scattering partner is a quasi-free parton.
3. The final state showers are passed backed to PYTHIA, which performs the hadronization of the showers.

JEWEL also generates the baseline p+p events analyzed in this thesis. Here, in the absence of a medium, the parton shower is simply treated as a vacuum parton shower when handed from PYTHIA to JEWEL.

Events are assigned a weight w that is related to the observed jet quenching, with highly quenched events being assigned a higher weight than those with lower quenching. This approach has the advantage that it reduces computation time by decreasing the statistics required to observe the same number of events with a large suppression of high p_{T} hadrons.

3.3 Recoil Partons

The medium in JEWEL is modeled as a distribution of quasi-free partons in space-time. When a jet interacts with a scattering center, a recoiling parton is generated along with the modified jet. By default, the hadrons generated by this recoiling parton are excluded from the final output of the event generator. However, JEWEL also provides the option of including these hadrons in the final event.

In this thesis, events including recoil hadrons are denoted by “recoil flag on", and events excluding them by “recoil flag off." Events where no QGP is produced are denoted by a “vacuum" label.

Like most Monte Carlo models for jet quenching, JEWEL has a region of validity in energy and momentum where pQCD can describe the interactions. Since any further soft interactions of the recoil particles with the medium typically

occur in a regime not described by perturbation theory, the recoil particles in JEWEL do not undergo further rescattering before hadronization. While this still allows the model to accurately describe the interactions of the jet with the medium, it does not describe the full event.

It is also important to note that the scattering centers are generated with non-zero net momentum. The p_{T} of the quasi-free partons is sampled from a thermal distribution, leading to fluctuations in the net p_{T} about zero. This is a notable effect, since when a jet interacts with a scattering center, the original scattering center is not removed from the medium. Thus, while momentum and energy conservation are strictly enforced at each vertex, the total final transverse momentum of all tracks in the event is not zero, with the remaining net momentum corresponding to the net momentum of the original scattering centers.

4 Results

4.1 Validating JEWEL

We begin by replicating some of the results of JEWEL presented in [3] to further validate the model. In particular, we study the event asymmetry, and both charged hadron and jet R_{AA}, for Pb+Pb events where recoil partons are and are not included (denoted by “Recoil on" and “Recoil off", respectively), and for p+p events (“Vacuum").

4.1.1 Asymmetry

One way to quantify the extent of jet quenching is through the asymmetry in the transverse momentum between the two leading (highest) momentum jets produced by a hard scattering. To study this asymmetry, define dijet events as in [1] by the following requirements:

1. Transverse momentum $p_{\mathrm{T}}^1 > 120\,\mathrm{GeV}/c$ and $p_{\mathrm{T}}^2 > 50\,\mathrm{GeV}/c$.
2. Pseudorapidity $|\eta^{1,2}| < 1.6$.
3. Azimuthal angle difference $|\Delta\phi^{12}| > \frac{2}{3}\pi$.

with $1,2$ denoting the leading and subleading jets, respectively. All charged tracks with $p_{\mathrm{T}} > 0.15\,\mathrm{GeV}/c$ were included in the jet finding. The asymmetry factor of a dijet event is defined as

$$A_J = \frac{p_{\mathrm{T}}^1 - p_{\mathrm{T}}^2}{p_{\mathrm{T}}^1 + p_{\mathrm{T}}^2}. \tag{4.1}$$

The asymmetry distributions for recoil on, recoil off and vacuum events are shown Figure 4.1. A cone radius of $R = 0.4$ was used in the jet finding. The results verify that Pb+Pb events are more likely to have larger asymmetry factors than p+p events. This suppression is evidence that the quenched jet will radiate a fraction of its energy at large angles relative to the leading jet axis. It is expected that increasing the jet radius would cause the subleading jet to recover the lost momentum, and would cause the distribution to recover its peak at $A_J = 0$. We note no significant difference between recoil on and off events. Furthermore, the distributions are in good qualitative agreement with those in [3].

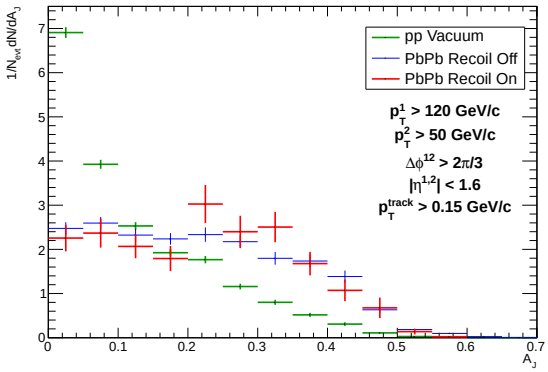

Figure 4.1: Asymmetry distributions of dijet events where hadron recoil particles are and are not included (denoted by “Recoil on" and “Recoil off", respectively), and for vacuum pp events (“Vacuum") where no quark-gluon plasma is produced. Jet finding was performed with a radius of $R = 0.4$, for all charged tracks with $p_{\mathrm{T}} > 0.15\,\mathrm{GeV}/c$.

4.1.2 Charged Hadron R_{AA}

We compute R_{AA} for charged hadrons as a function of $p_{\mathrm{T}}^{\mathrm{track}}$. We include tracks with transverse momentum $p_{\mathrm{T}}^{\mathrm{track}} > 5\,\mathrm{GeV}/c$, and pseudorapidity $|\eta^{\mathrm{track}}| < 2.4$. Following [3], we analyze events including recoil hadrons, in addition to

recoil off. The results are presented in Figure 4.2a.

The suppression of high p_T hadrons due to jet quenching is clearly evident in the values of R_{AA} below unity. Comparing recoil on and recoil off events, we note no significant difference between the R_{AA} values at high $p_T^{track} > 10\,GeV/c$. At low $p_T^{track} < 10\,GeV/c$, we find that the recoil on events have a peak at low p_T as compared to the recoil off. This suggests that the recoil tracks have a soft p_T distribution.

To compare, the charged hadron R_{AA} from [3] is presented in Figure 4.2b. While comparison of the two at high $p_T^{track} > 100\,GeV/c$ is complicated by available statistics, there is a good agreement for $p_T^{track} < 100\,GeV/c$. In [3], R_{AA} crosses unity at $p_T^{track} \approx 300\,GeV/c$, compared to our analysis which crosses unity at $p_T^{track} \approx 200\,GeV/c$. The slight discrepancy in these values can be accounted for by statistical uncertainties. The trend toward unity has also been verified by experimental data also shown in Figure 4.2b. It should be noted, however, that the increase above $R_{AA} = 1$ is likely a generic feature of the model, rather than a product of of the underlying physics in the event.

4.1.3 Jet R_{AA}

As a further validation of JEWEL, we compute R_{AA} for jets as a function of p_T^{jet}. To compare to [3], we do so for events where recoil particles are excluded from the final output.

We make a cutoff in the selection of tracks used in jet finding in $p_T^{track} > 0.15\,GeV/c$. Furthermore, we follow [7] in making a cutoff for jets found in momentum $p_T^{jet} > 5\,GeV/c$ and pseudorapidity $|\eta^{jet}| < 0.5$. In Figure 4.3, the yields of Pb+Pb events are shown for different cone radii.

Plots of R_{AA} as a function of cone radius are shown in Figure 4.4. We find that the approximate value of $R_{AA} \approx 0.2$ agrees well with the results presented for the model for cone radii $R = 0.2, 0.3$, shown in Figure 4.5 [3].

However, as discussed in Section 2.1, the theoretical expectation is for the factor to increase slightly with increasing jet $p_\perp$, as also observed in the experimental data presented by ALICE in Figure 4.5. Contrary to this, we observe no dependence on $p_\perp$. Furthermore, as discussed in Section 2.2, we expect the factor to depend on the cone radius used in the jet finding. Again, we observe no dependence on the cone radius.

One explanation for this discrepancy is the exclusion of recoiling hadrons from the analysis. In the limit when the cone radius includes all tracks in the event, no momentum is lost by the jet, and so theoretically for all p_T bins $R_{AA} = 1$. However, without recoil hadrons, the momentum lost by tracks in quenched events is not recovered by an increasing cone radius in Figure 4.4. Evidently, recoil hadrons represent a significant part of the interaction of the jet with the medium, and excluding these hadrons does not allow for the complete event to be studied.

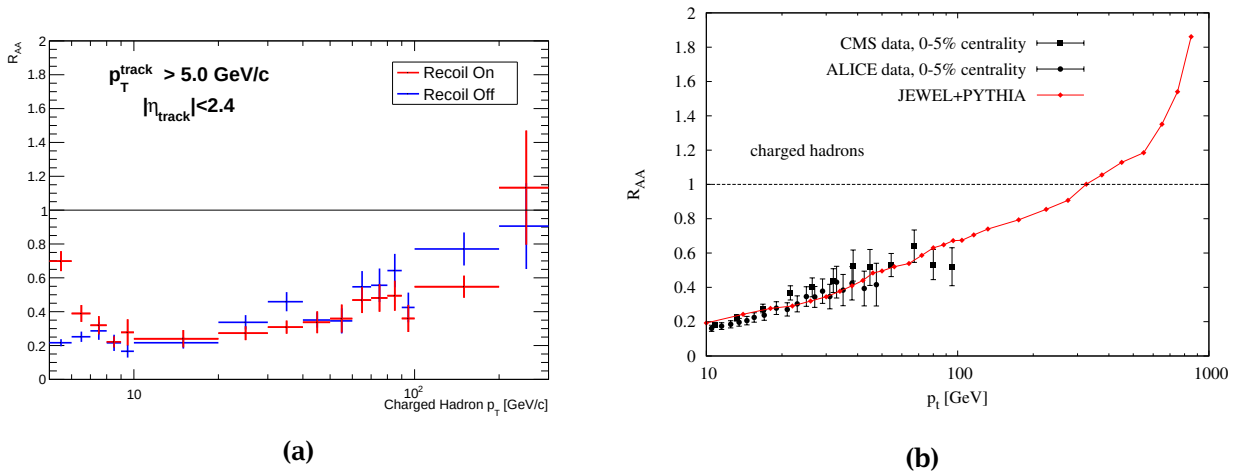

(a) **(b)**

Figure 4.2: (a) Charged hadron R_{AA} for recoil on and recoil off events. Cutoffs are made in track selection of $p_{\mathrm{T}}^{\mathrm{track}} > 5\,\mathrm{GeV}/c$ and $|\eta^{\mathrm{track}}| < 2.4$. **(b)** Charged hadron R_{AA} as presented in [3], for comparison. Both MC results from JEWEL and experimental data from the ALICE and CMS collaborations are shown.

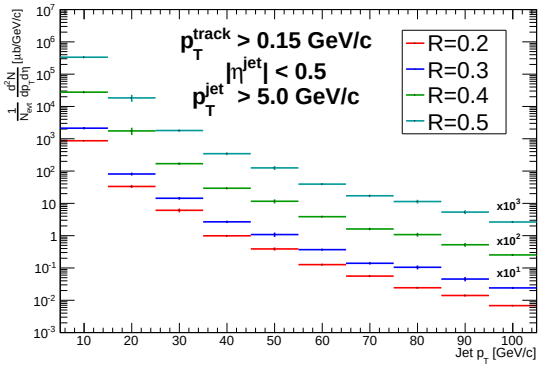

Figure 4.3: Yields for events where hadron recoil is not calculated, as a function of cone radius. Cutoffs are made for tracks $p_{\mathrm{T}}^{\mathrm{track}} > 0.15\,\mathrm{GeV}/c$ and jets $p_{\mathrm{T}}^{\mathrm{jet}} > 5\,\mathrm{GeV}/c$ and $|\eta^{\mathrm{jet}}| < 0.5$.

4.2 Momentum Conservation

The independence of jet R_{AA} in Figure 4.4 in events where recoil hadrons are excluded indicates that the momentum lost by the quenched jets is not recovered by other tracks in the event. We postulate that the lost momentum must be carried away by the recoil hadrons. To confirm this hypothesis, we compare the momentum balance in events including and excluding recoil particles.

Consider dijet events as defined above, where no cutoffs have been made for track p_{T}. For all tracks in the event, compute the projection of the track p_{T}^{i} onto the leading jet axis as

$$p_{\mathrm{T}}^{||} = \sum_i -p_{\mathrm{T}}^{i}\cos(\phi^i - \phi^1), \qquad (4.2)$$

where ϕ^1, ϕ^i are the azimuthal angles of the leading jet and track, respectively. The weighted average of these sums over events is

$$< p_{\mathrm{T}}^{||} >= \frac{\sum_j w_j p_{\mathrm{T},j}^{||}}{\sum_j w_j}, \qquad (4.3)$$

where w_j is the weight of the event. We excluded events with a weight $w_j > 1.0\times10^{-10}$. The effect of this cutoff is both to limit the

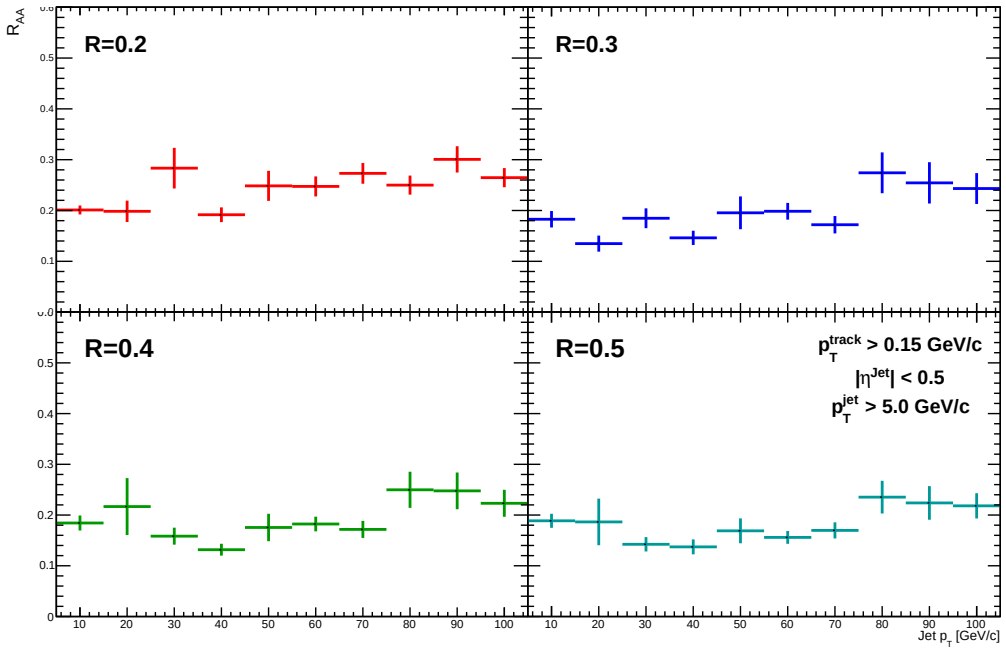

Figure 4.4: Jet R_{AA} computed from the yields in Figure 4.3, for events where recoil hadrons are excluded, as a function of cone radius.

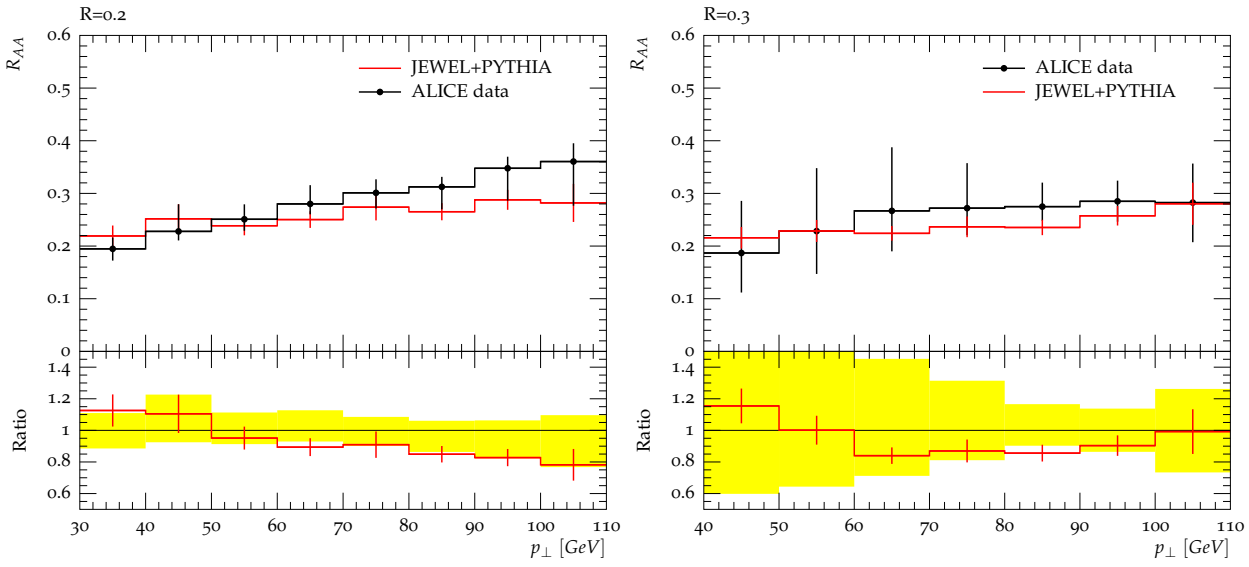

Figure 4.5: Jet R_{AA} from [3], for both MC data from JEWEL and experimental data from ALICE. Ratios for comparison to experimental data are also included.

computing time, and to eliminate high weight events from dominating the analysis.

Figure 4.6 shows the average transverse momentum $< p_{\mathrm{T}}^{||} >$ as a function of the event asymmetry A_J and track transverse momentum. For events where recoil hadrons are excluded, there is a strong momentum imbalance toward the leading jet. Conversely, including recoil hadrons restores the momentum balance to great extent, although the average event continues to have a net projected momentum imbalance of several GeV/c.

Comparing these results to those presented in [1], as shown in Figure **??**, there is a notable similarity in that a larger fraction of high $p_{\perp} > 8.0$ GeV/c tracks is found in the leading jet hemisphere than the subleading, while a larger fraction of soft $p_{\perp} < 8.0$ GeV/c tracks is found in the subleading jet hemisphere than the leading. This qualitatively good agreement to data improves upon the results of previous MC models such as PYTHIA+HYDJET, as shown in Figure 4.7.

To determine the radial dependence of the momentum balance, the projected momentum inside and outside a cone around the leading jet axis is shown in in Figure 4.8. Following [1], a cone radius of $\Delta R = 0.8$ was used in the analysis.

When hadron recoil is not calculated, the JEWEL results resemble the PYTHIA+HYDJET model presented in Figure 4.9, in that a dominant (> 50%) contribution in the out-of-cone radiation is carried by tracks with $p_{\perp} > 4$ GeV/c. Turning the recoil flag on significantly increases the contribution of low $p_{\perp} < 2$ GeV/c to the momentum balance, a feature of the experimental data presented by the CMS collaboration. This increase is present in both the in-cone and out-of-cone radiation, but more dominantly in the latter, for high A_J events. The soft p_{T} distribution of recoil tracks radiated at large angles to the leading jet axis suggests that the recoil hadrons resemble a background, similar to the underlying event in experimental Pb+Pb collisions.

Despite the effect that including recoil hadrons has on the momentum balance, the residual imbalance of several GeV/c is a point of concern. The distributions of the projected momenta for events including and excluding hadron recoils and for p+p vacuum events are plotted in Figure 4.10. The effect of including hadron recoils is reflected in the shift in the average of the distribution toward zero. However, while p+p events have a narrow distribution in momentum balance, Pb+Pb events with recoil on have a significant spread in net momentum. As described in Section 3.3, this remaining net momentum is the non-zero net momentum of the original scattering centers generated in the medium, due to the fact that the parton energies are sampled from a thermal distribution. Since JEWEL does not model the full event, but only interactions of the jet with the medium, this original net momentum remains in the final state particles generated.

Nonetheless, it is evident that it is necessary to include recoil hadrons in analyses that depend on momentum conservation. Furthermore, including them presents a more complete description of the whole event, particularly of parton showers that are produced outside the leading and subleading jets.

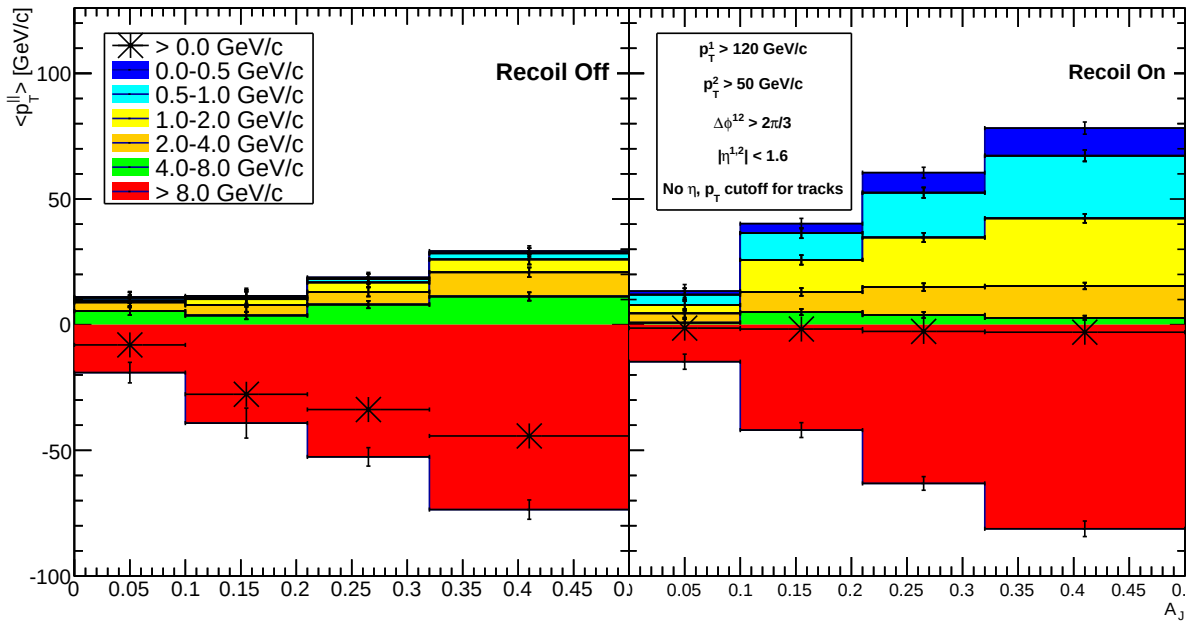

Figure 4.6: Average projected transverse momentum onto the leading jet axis, for events where recoil hadrons are excluded (left) and included (right). No cutoffs were made for tracks in transverse momentum nor pseudorapidity. Contributions to the total is also shown in track p_{T} bins. Statistical uncertainties represented by vertical bars are calculated as the standard deviation of the weighted average $< p_{\mathrm{T}}^{||} >$ for each A_J, p_{T} bin.

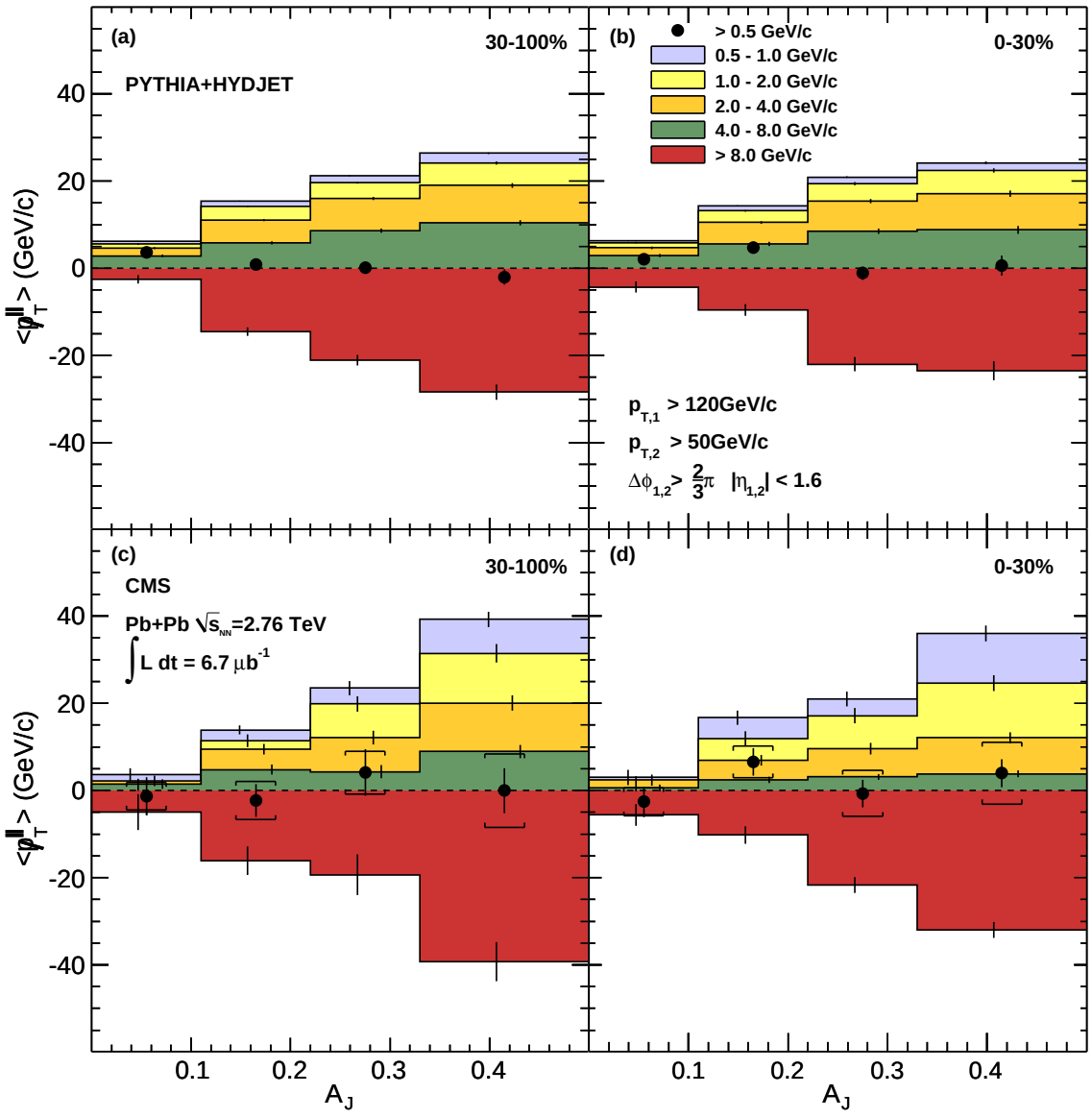

Figure 4.7: Data from the CMS collaboration (bottom), and from a PYTHIA+HYDJET MC model (top), for the average projected transverse momentum onto the leading jet axis [1].

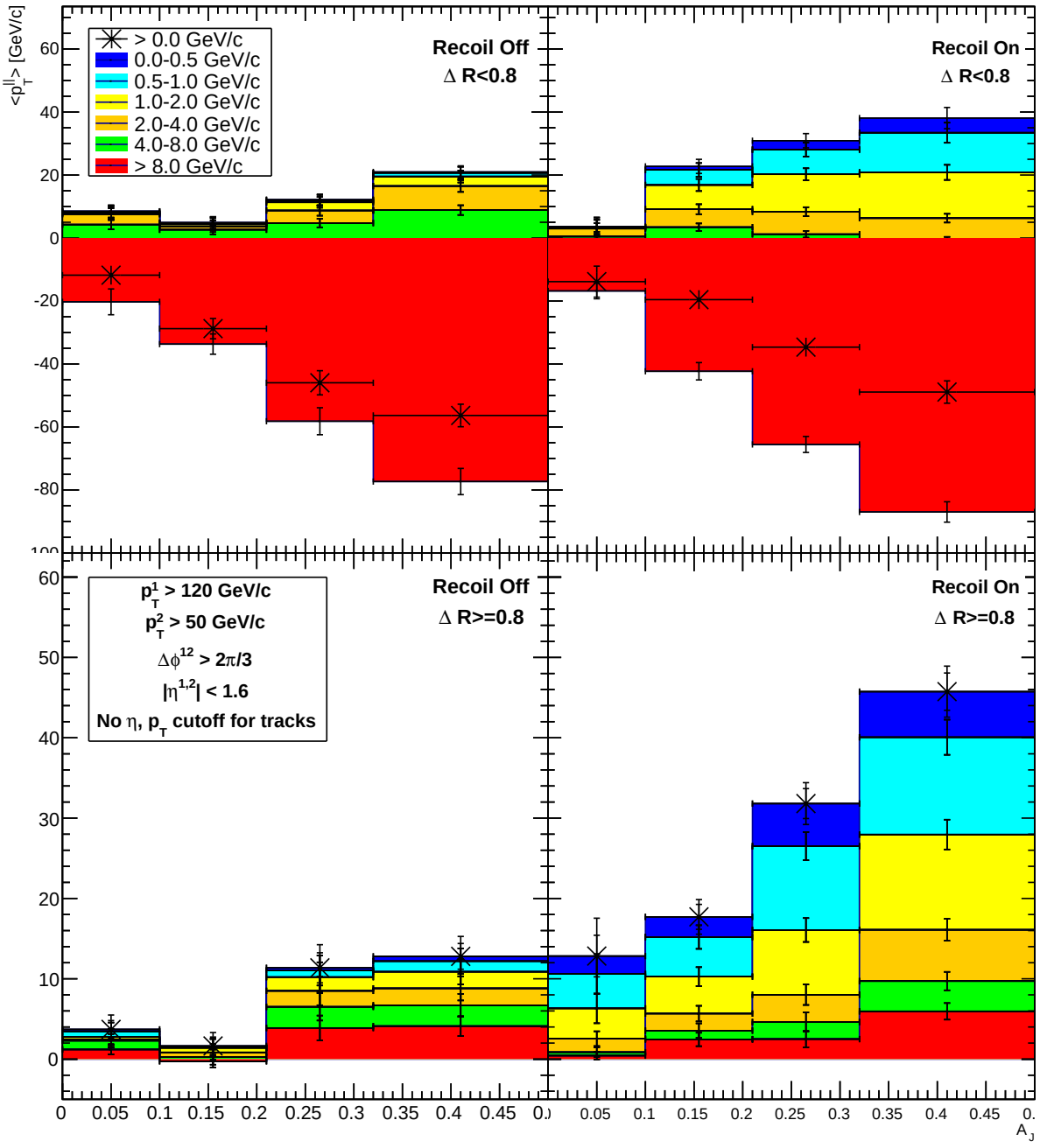

Figure 4.8: Average projected transverse momentum inside and outside a cone of radius $\Delta R = 0.8$ around the leading jet axis. No cutoffs were made for tracks in transverse momentum nor pseudorapidity. Statistical uncertainties represented by vertical bars are calculated as the standard deviation of the weighted average $< p_{\perp}^{||} >$ for each A_J, $p_{\perp}$ bin.

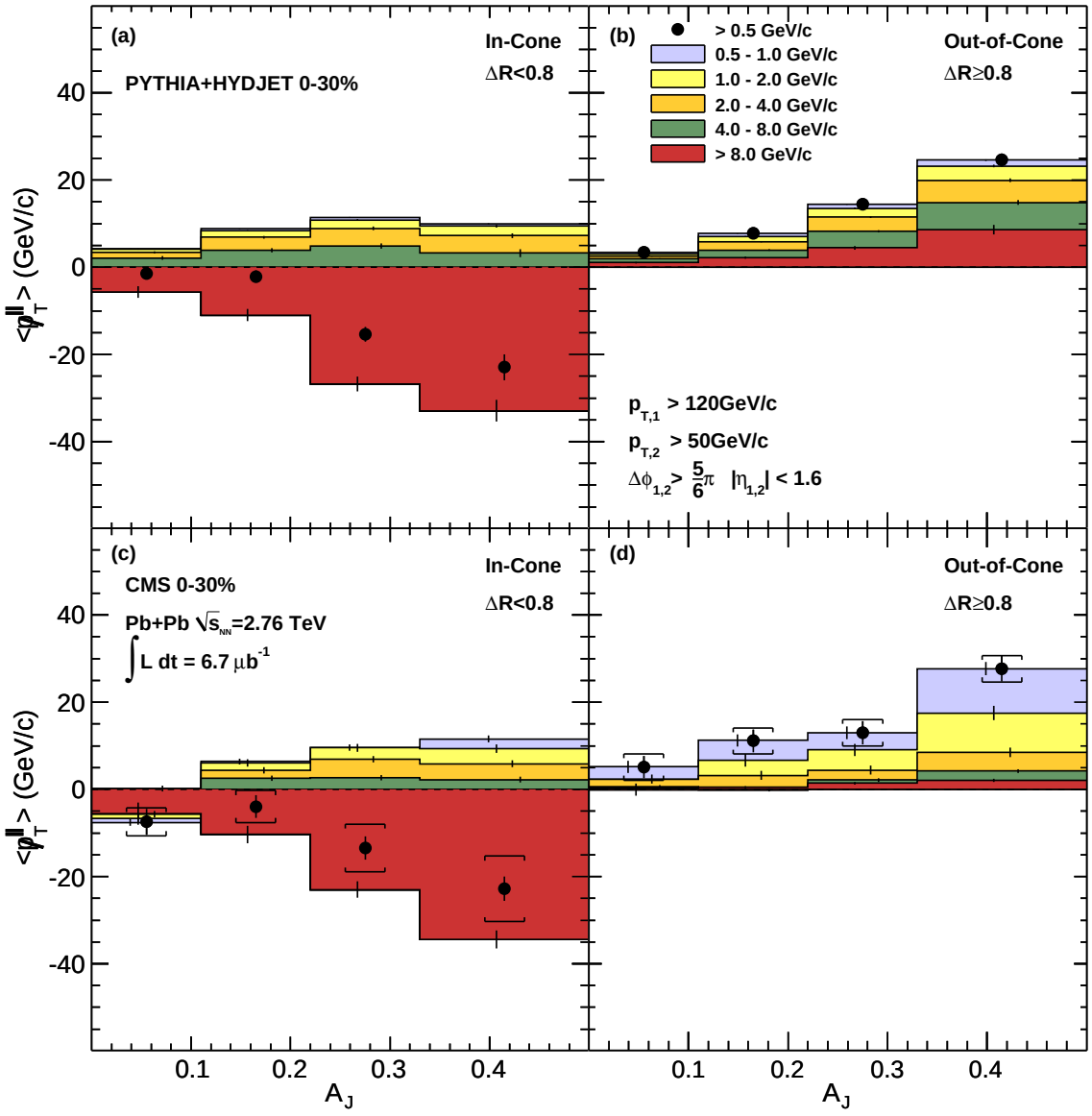

Figure 4.9: Data from the CMS collaboration (bottom), and from a PYTHIA+HYDJET MC model (top), for the average projected transverse momentum inside and outside a cone of radius $\Delta R = 0.8$ around the leading jet axis [1].

4.3 Background Subtraction of Recoil Hadrons

There exists a residual uncertainty when comparing JEWEL results to data, since the MC procedure for modeling the event is not the same as in experiment. In particular, JEWEL only models the interactions of the jet with the medium, and does not simulate the whole event. In high energy experimental data for Pb+Pb collisions, the final state particles are products of both hard nucleon-nucleon collisions that produce high p_{T} jets, and the underlying event, composed mainly of soft interactions that occur in the medium. In order to study the momentum of the jets in the absence of the underlying event's contribution, it is necessary to perform a background subtraction of the underlying event from the reconstructed jets p_{T}.

Similarly, recoil partons in JEWEL resemble the underlying event. Events where recoiling hadrons are included typically have $O(10)$ more tracks per event than the vacuum p+p events in the same area in the ϕ, η plane. Without background subtraction, each reconstructed jet has a contribution to its p_{T} from the underlying event, and the distribution of the yields of jets $\frac{d^2N^{\mathrm{AA}}}{dp_{\mathrm{T}}d\eta}$ is shifted toward higher p_{T}, leading to $R_{\mathrm{AA}} >> 1$. This effect is particularly evident for large cone radii $R \gtrsim 0.3$, as each jet will have an even greater contribution from the underlying event than for small radii. Furthermore, the recoil tracks soft p_{T} distribution suggests that they may be a part of what in experiment would be considered a background.

Therefore, we propose to include recoil hadrons in our analysis by assessing the p_{T} of the recoil tracks that are not correlated with the jet by performing background subtraction from the reconstructed jets. This has the advantage that the analysis procedure more closely resembles the experimental, and that the results represent a more complete description of the event by including the recoil hadrons.

We follow the same method of background subtraction as in experiment, described in detail in [13]. For a jet i, in the ϕ, η plane we choose some region $\mathfrak{R}$ about i to sample $\rho^i_{\mathfrak{R}}$, the jets transverse momentum density of the background under the jet, defined as

$$\rho^i_{\mathfrak{R}} = \mathrm{median}\left\{\frac{p^j_{\mathrm{T}}}{A^j}\right\}_{j\in\mathfrak{R}}, \tag{4.4}$$

where A^j is the area of each jet in the region for $j \neq i$. The background subtracted transverse momentum $p^{i,\mathrm{sub}}_{\mathrm{T}}$ of each jet in the event can then be calculated from the original momentum $p^{i,\mathrm{full}}_{\mathrm{T}}$ as

$$p^{i,\mathrm{sub}}_{\mathrm{T}} = p^{i,\mathrm{full}}_{\mathrm{T}} - \rho A^i. \tag{4.5}$$

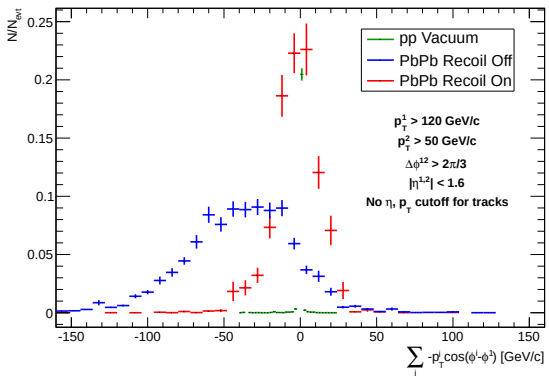

Figure 4.10: Distributions of projected transverse momenta for Pb+Pb recoil on, recoil off and p+p vacuum events.

To determine the region to sample the background density from, we examine the distributions of tracks in η, ϕ for events where recoil hadrons are included compared to those where they are excluded. In a single event, the recoil hadrons are expected to cluster around the high p_T jets that formed them. Since in a broad interval around mid-rapidity, the leading and subleading jets have no preference for orientation in η nor ϕ over many events, then recoil hadrons are as well expected to be evenly distributed in the η, ϕ plane.

As expected, the distributions of tracks for recoil on and recoil off events flat in ϕ. However, the distribution in η is peaked around $\eta = 0$ for events where recoil hadrons are included, compared to a flat distribution for recoil off events, as shown in Figure 4.11. This distribution of recoil hadrons raises several questions regarding how recoil particles are generated, and requires further discussion.

4.3.1 Distribution of Recoil Hadrons in Pseudorapidity

One particular curiosity of JEWEL is the generation of recoil hadrons in η. In Figure 4.12, the distributions of charged track η values are shown for events with and without recoil hadrons. The additional tracks in the former contribute to a peak around $\eta = 0$, which is not present in the latter. The diminishing peak with increasing track p_T can be accounted for by the fact that recoil particles are the result of soft interactions between the jet and the medium, and therefore dominantly populate low p_T bins. The peak in the distribution at high p_T in events where recoil particles are excluded can be attributed to low statistics.

In comparison, in Figure 4.13 the charged track η distributions from experimental data from various collaborations is presented, taken from [14]. There is noticeably no peak around $\eta = 0$ as found in JEWEL. This poses the question of why modeling more of the full event in JEWEL should lead to a less uniform track distribution in η.

It may be postulated that the distribution is a result of color connection between partons produced by the hard scatterings that influence a tracks location during hadronization. This would indicate a connection between high p_T tracks and recoil tracks. However, Figure 4.14 shows the track distributions in ϕ, η for four representative recoil flag on events where the lead p_T track is at pseudorapidity $|\eta| > 2$. Despite the relatively high η of the lead track, the recoil hadrons are consistently generated in a strip around $\eta = 0$, rather than clustered around the track.

This effect is assessed over many events in Figure 4.15. Track $\Delta\eta$ values are plotted for various bins in $|\eta|$ of the lead p_T track. For recoil flag off events, the distributions show that regardless of in which η bin the lead track is generated, a small peak of tracks are produced about it in η. Conversely, in recoil flag on events, lead tracks produced at high $\eta > 2$ do not have recoil hadrons produced about the track, but rather at constant distance away in $\Delta\eta$. The slight asymmetry between the peaks in $\pm\Delta\eta$ for the lead track $\eta > 2.5$ is attributed to low statistics.

These results can be summarized in two main points of interest:

1. Recoil hadrons are generated in a strip of constant width about $\eta = 0$. This presents a discrepancy to the experimental data in 4.13.

2. Recoil hadrons are generated in η independent of the jets orientation in ϕ, η. This is particularly evident in the rare events in which high p_T tracks are generated at high η, where the recoil hadrons are still generated in a strip about constant $\eta = 0$.

4.3.2 Regions for Sampling the Recoil Background

We wish to assess the median jets transverse momentum density for recoil tracks that are not correlated with each jet in the event. In the background subtraction procedure described in [13], regions are chosen around the jet from

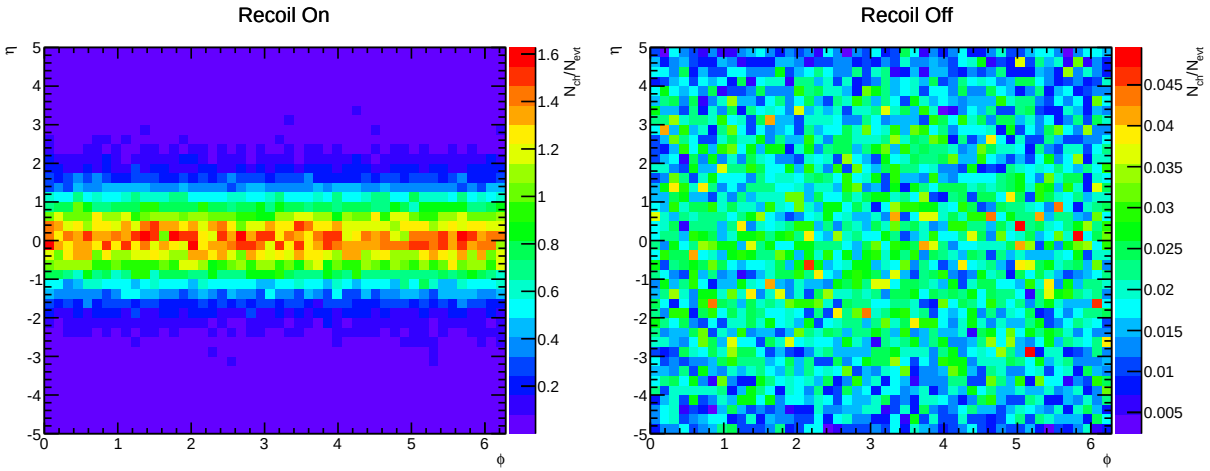

Figure 4.11: Average distribution of tracks for events where recoil hadrons are included (left) and excluded (right). No cutoff is made for the tracks in p_{T}.

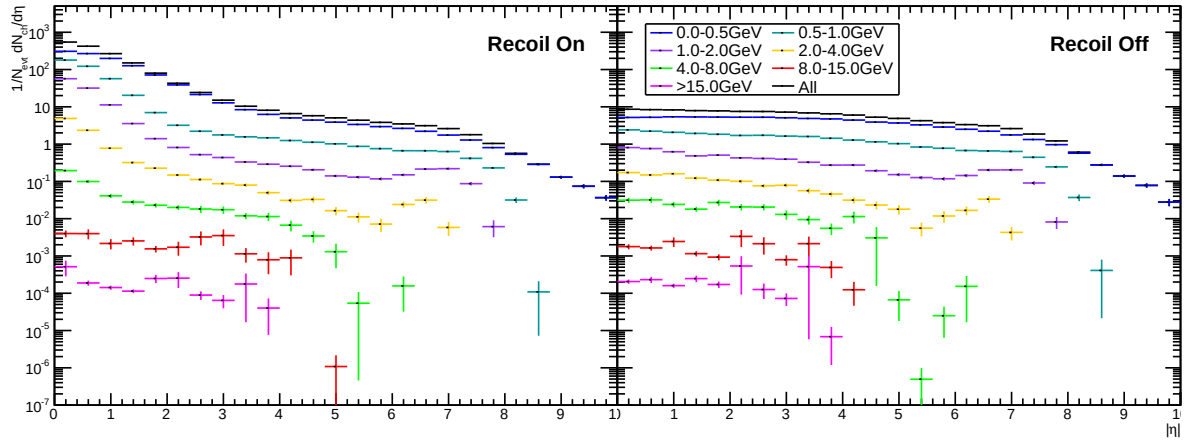

Figure 4.12: Distributions of track η for various p_{T} bins, for events where recoil hadrons are included (left) and excluded (right).

which the background is calculated; that is, the background density differs for different jets in the event. We propose a simpler model, choosing a strip region S in η that is based on the distribution of recoil tracks, leading to a single ρ value per event.

We define the following four regions to compare:

$$S_{2R} : |\eta| < 2R + 1.6$$
$$S_{0.5} : |\eta| < 0.5$$
$$S_{1.0} : |\eta| < 1.0$$
$$S_{2.0} : |\eta| < 2.0$$

In all regions, the leading and subleading jets are excluded from computing ρ, as these are typically of much higher p_{T} than the other jets in the event.

Figure 4.16 shows the weighted average over events of p_{T}/A in each η bin, for various jet radii. The width of the recoil "bump" in the distribution in η varies as approximately $|\eta| < 2R + 1.6$.

Choosing regions of constant η to sample that are independent of the jet in question leads to a discrepancy in that ρ does not represent the local background around the jet, but rather in the overall event. However, the analysis follows experimental cutoffs in [7] taking jets with $|\eta| < 0.5$ when calculating R_{AA}. From Figure 4.16, it is seen that jet p_{T}/A varies little in η in this region. Furthermore, the recoil tracks distribution in η opposes the theory that recoil partons are expected to be co-moving with the parton shower and hence generated about the jet. Therefore, it is unclear whether the location of a recoil track in η is correlated with the location of the jet in η. Hence, the strip regions of constant width proposed above are taken as an approximation of the background density.

Since the background is composed to recoil tracks that are independent of the jet finding radius used, we conjecture that ideally the background density $\rho_S(R)$ in the region S should also be independent of R. To compare the four regions sampled, compute the standard deviation σ_S over R values as

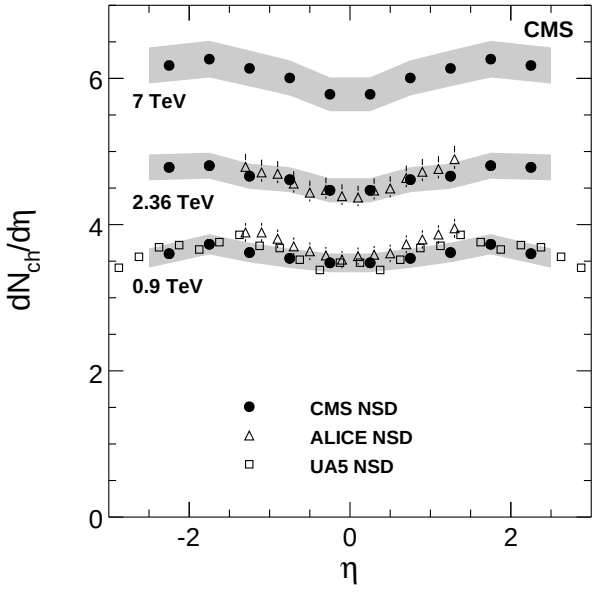

Figure 4.13: Experimental data from various collaborations for the distribution of track η values, taken from [14].

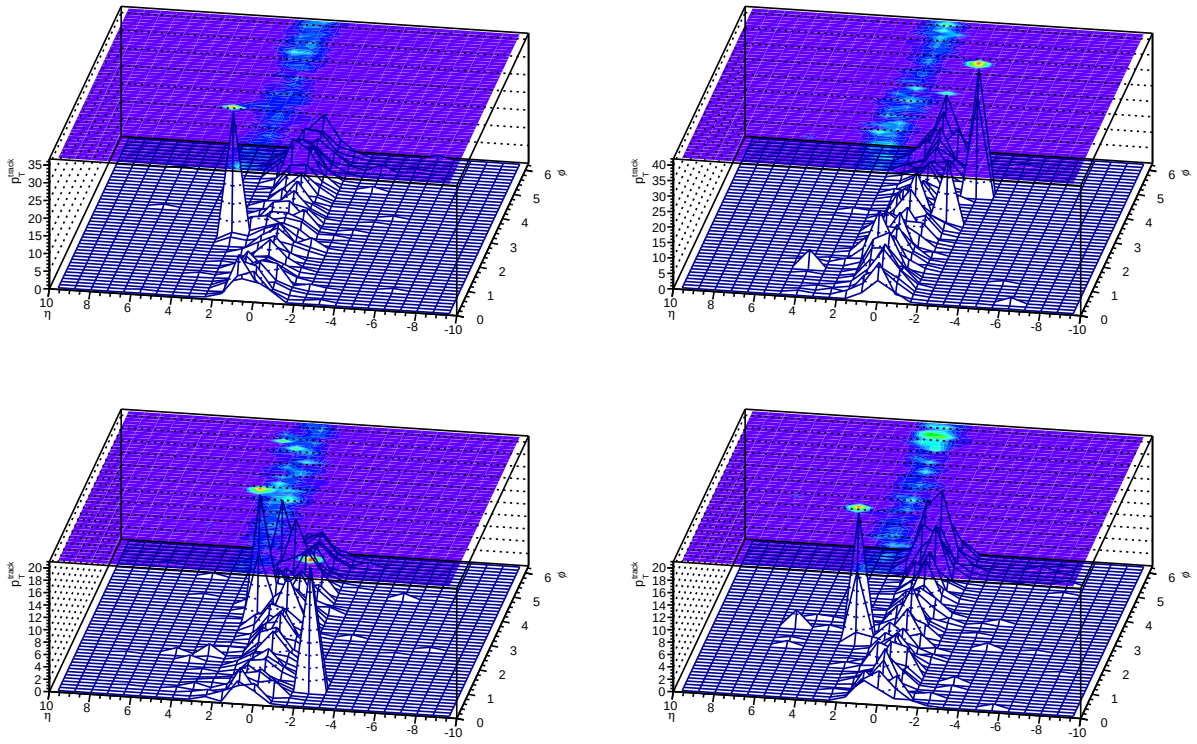

Figure 4.14: Track distributions in ϕ, η for four representative events where recoil hadrons are included and the lead p_{T} track is at pseudorapidity $|\eta| > 2$. No cutoff is made in track p_{T}.

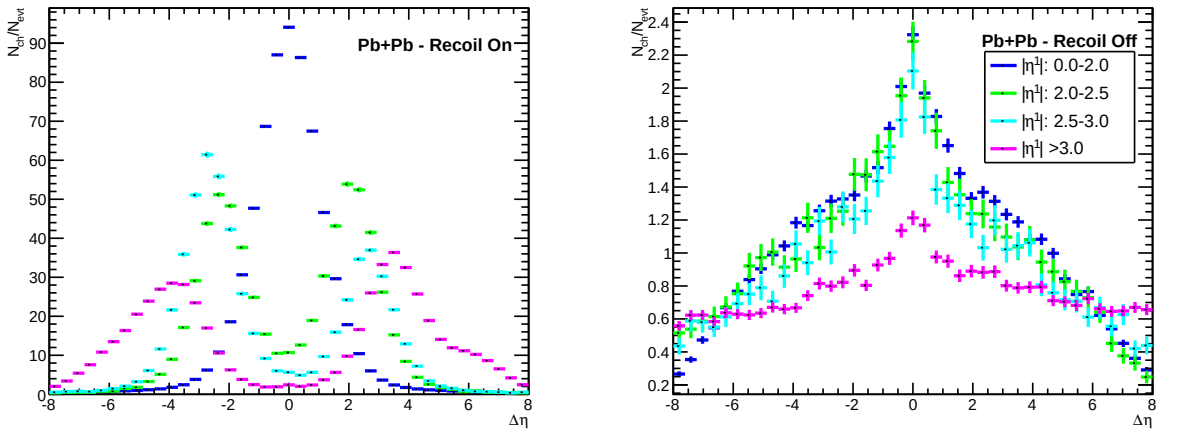

Figure 4.15: Distributions of $\Delta\eta$ for various $|\eta|$ bins of the lead p_{T} track in each event. Events including recoil hadrons are shown on the left, excluding on the right. No cutoff is made in track p_{T}.

$$\sigma_S = \sqrt{\frac{1}{N}\sum_{j=1}^{N}\left(\rho_S(R_j) - \mu\right)^2}, \qquad (4.6)$$

where R_j runs over the R values sampled, and μ is the average ρ_S.

Distributions of σ_S for the four regions sampled are shown in Figure 4.17. There is a clear distinction between the S_{2R} region's distribution and those of regions with constant width in η, which are more sharply peaked at lower σ. The three regions of constant width are compared by the average values and RMS of the distributions, as given in Appendix A. Since the $S_{1.0}$ region has both the lowest average value of $\sigma_{\text{ave}} \approx 1.588\,\text{GeV}/c$, and the lowest RMS value of $0.901\,\text{GeV}/c$, it is the best suited out of the four for sampling the background density. The distributions of ρ values from the $S_{1.0}$ region for various jet radii are shown in Figure 4.18.

4.3.3 R_{AA} after Background Subtraction

Figure 4.19 shows the spectrum of jet p_{T} for various cone radii. The region $S_{1.0}$ was used to sample the background density ρ. Without background subtraction, there is a clear shift in the distributions toward higher p_{T}. At very high p_{T}, the effect of jet quenching diminishes due to the kinematic effect described in Section 2.1. The net effect of these two tendencies is a "bump" in the yield toward high p_{T}, the

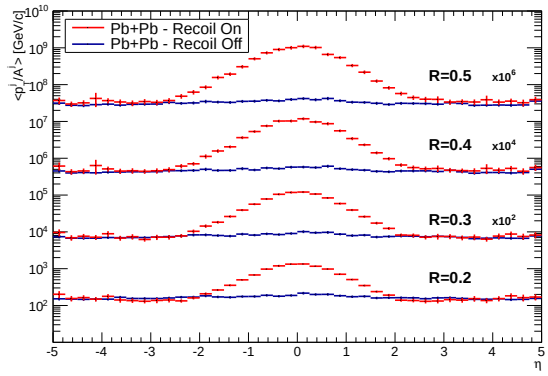

Figure 4.16: Jet p_{T}/A as a weighted average in each bin over events (denoted by $\langle p_{\text{T}}/A\rangle$), as a function of η, for various jet radii.

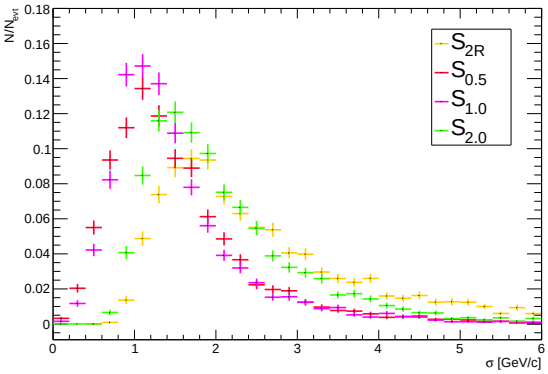

Figure 4.17: Distributions of σ values for the four regions sampled.

upper edge of which moves to higher p_T with increasing jet radius.

The background subtraction works to counter this bump, bringing the spectra below the vacuum p+p events. However, for very low p_T, the Pb+Pb distribution continues to stay above the p+p distribution. This may be a residual effect similar to the recoil off case, where low $p_T < 5\,\text{GeV}/c$ jets are found above the p+p distribution.

Furthermore, the p_T value at which the Pb+Pb distribution drops below the p+p increases with increasing cone radius. This may suggest that the "bump" in the full events grows faster with increasing jet radius than the p_T that is subtracted from the jet, i.e. ρA. However, the amount that the "bump" grows by with increasing radius is also related to the area A, although the density of jet p_T/A is not constant in η, as shown in Figure 4.16.This may suggest that when choosing the region to compute the ρ values, the optimal choice may not be the region with the most radius-independent values.

Figure 4.20 shows the jet R_{AA} for various cone radii. While at low radii events without background subtraction have factors below unity, for radii $R > 0.3$ we find an unphysical increase, due to the increased number of tracks in the event that are grouped into a single jet. Subtracting a background from these jets re-

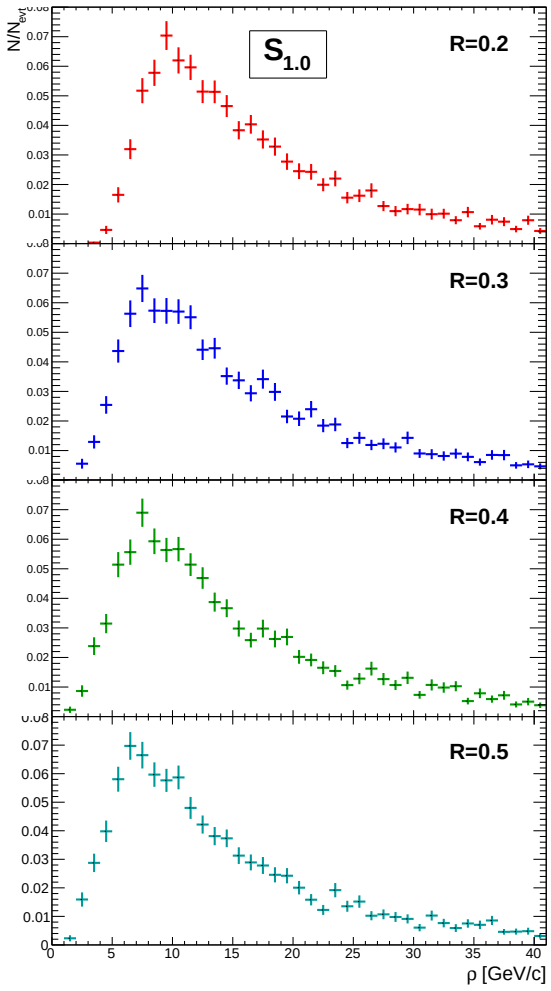

Figure 4.18: Distributions of ρ values for various jet radii, for the $S_{1.0}$ region.

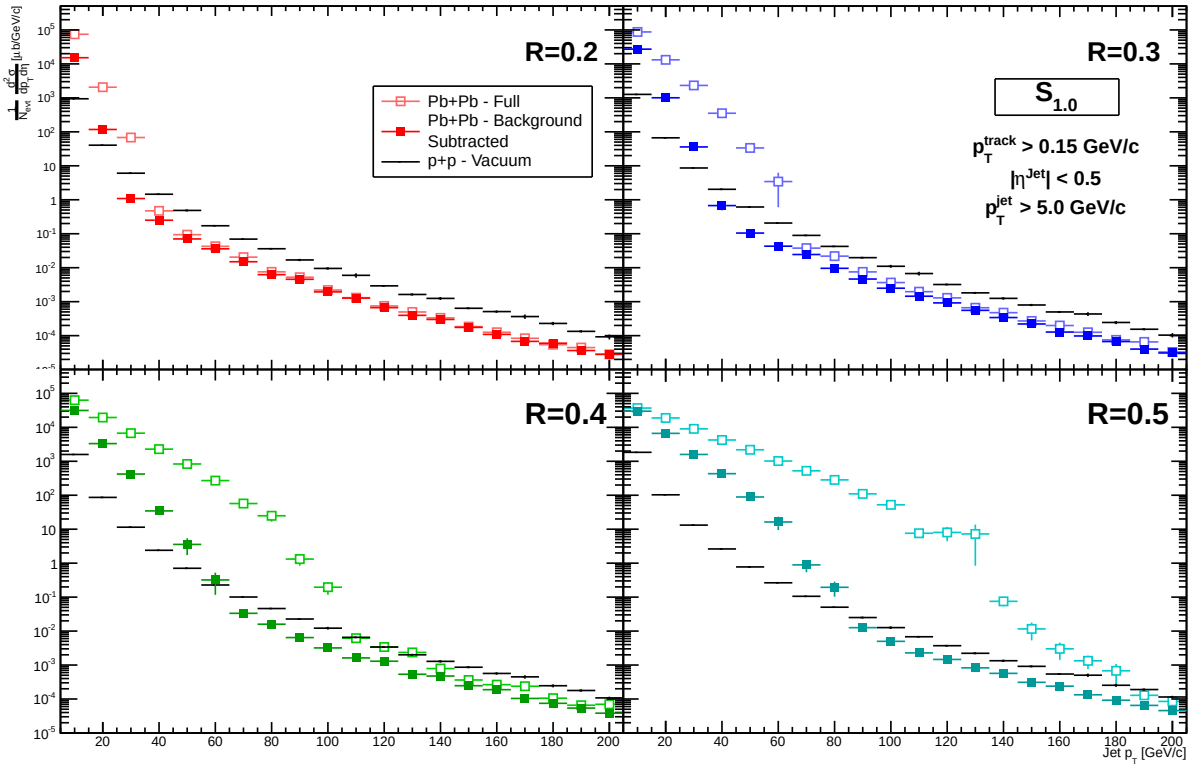

Figure 4.19: Yields of jet p_{T} found for various jet radii, for the full (no background subtraction) and background subtracted jets. ρ values were sampled from the $S_{2.0}$ region. Cutoffs were made in track $p_{\mathrm{T}} > 0.15\,\mathrm{GeV}/c$ and jet $|\eta| < 0.5$ and $p_{\mathrm{T}} > 5.0\,\mathrm{GeV}/c$.

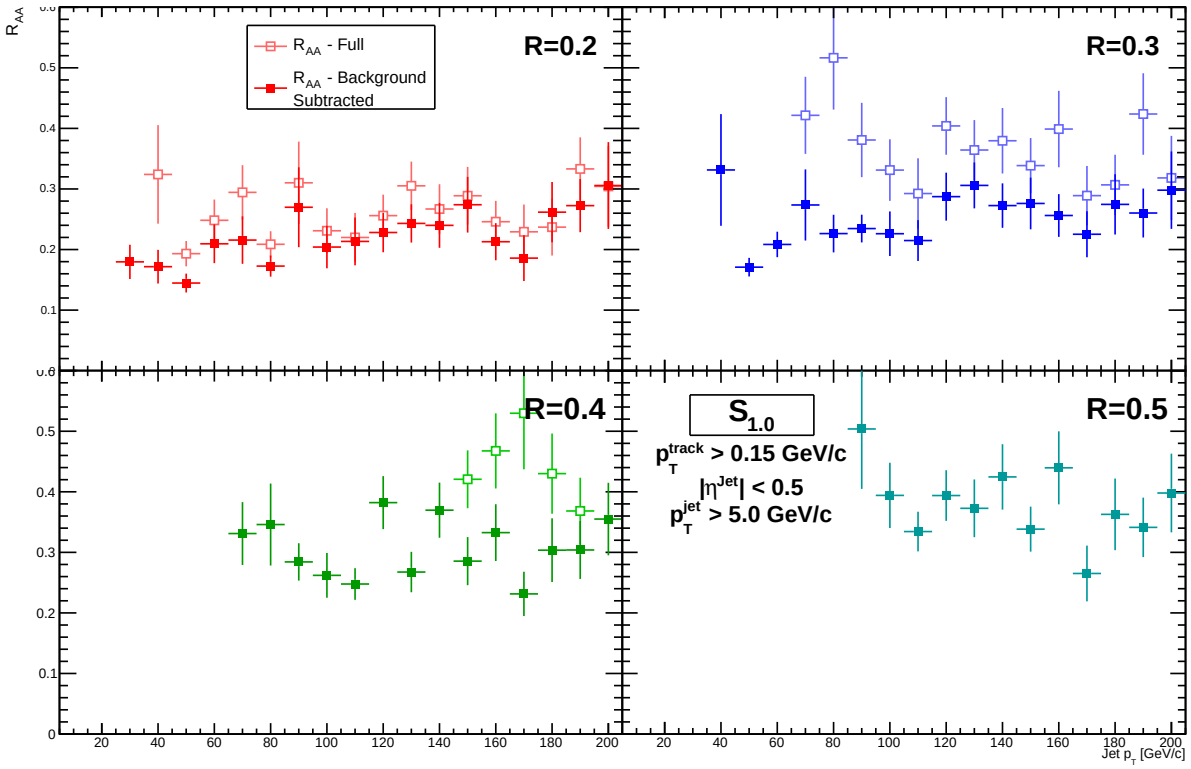

Figure 4.20: Jet R_{AA} calculated from the cross sections in Figure 4.19, using the same cutoffs. At low p_{T}, $R_{\mathrm{AA}} > 1$ (not shown).

covers the R_{AA} to below unity. The point at which the Pb+Pb distribution drops below the p+p can be clearly seen by where $R_{AA} < 1$ at various radii.

In Figure 4.5, experimental data for R_{AA} from the ALICE experiment is presented. For a radius of $R = 0.2$, the factor increases from $R_{AA} \approx 0.2$ at jet $p_T = 30\,\text{GeV}/c$ to $R_{AA} \approx 0.38$ at $p_T = 100\,\text{GeV}/c$. For a radius of $R = 0.3$, the increase is not as evident due to statistical errors, but can be estimated as $\Delta R_{AA} < 0.1$ over approximately the same range in p_T. While the JEWEL data presented in Figure 4.5 is calculated for events where recoil hadrons are excluded, approximately the same results are obtained for $R = 0.2, 0.3$ in Figure 4.20. For $R = 0.2$, an increase from $R_{AA} \approx 0.2$ at $p_T = 30\,\text{GeV}/c$ to $R_{AA} \approx 0.3$ at $p_T = 200\,\text{GeV}/c$ is observed.

At higher radii, however, no clear dependence on jet p_T is observed. It is possible that this is due to the increase to higher p_T of the cutoff at which R_{AA} drops below unity with increasing R. Experimental data in [3] from ALICE hints that the dependence on jet p_T decreases with increasing jet radius.

The magnitude of the shift in R_{AA} due to an increasing jet radius is now clearly visible. As shown in Figure 4.21, the average value over jet p_T bins increases with increasing jet radius, due to the recovered momentum from the recoil tracks. It is ambiguous whether the rate of increase depends on the radius R. Furthermore, it must be noted that there is an uncertainty in comparing $R_{AA} > 1$ values, as the shift in the drop of the p+p distribution below the Pb+Pb distribution as shown in Figure 4.19

Furthermore, the plots in Figure 4.21 show that the background subtracted R_{AA} greatly depend on the region sampled. While the results of jet analysis in both MC and experiment greatly vary with algorithm and cone radius used, the background subtraction procedure introduces another factor of uncertainty.

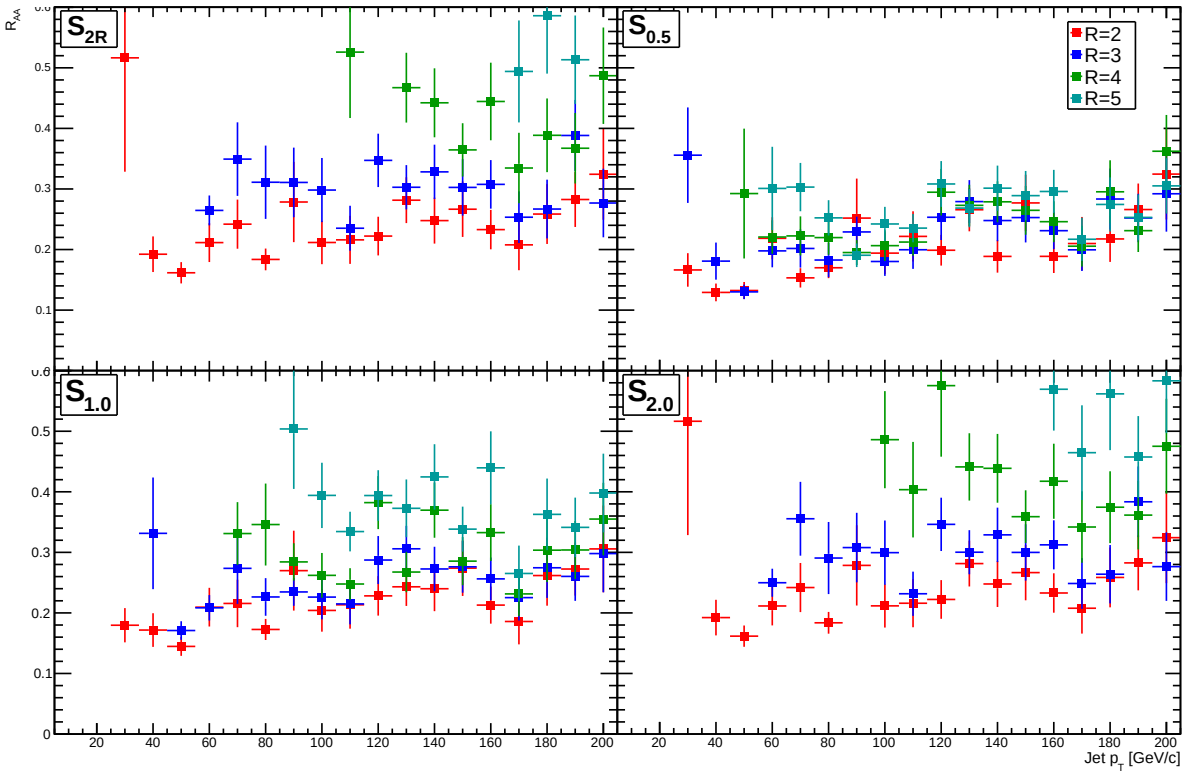

Figure 4.21: Jet R_{AA} calculated for background subtracted jets, to compare for various radii, for all four regions sampled. The same cutoffs were used as in Figure 4.20.

5 Discussion

Hard probe observables of jet quenching in JEWEL agree qualitatively well with experimental data. However, several unresolved issues and limitations remain. In particular, comparing Monte Carlo models of jet quenching to experiment presents a residual uncertainty in that the MC does not model the full event. Not only does this remove some of the description of the underlying physics in the event, but the analysis procedures also differ.

JEWEL focuses on modeling only the interactions of the jet with the medium. The limitations of this method is seen in the R_{AA} for recoil flag off events in Figure 4.4, where the suppression found is independent of the cone radius employed in the jet finding. Furthermore, momentum and energy are conserved at each vertex in the simulation, but excluding recoil tracks causes an average net momentum imbalance of $\approx 45\,\mathrm{GeV}/c$, as seen in Figure 4.10.

Observables based on the recoil off flag are inherently limited by their momentum imbalance. On the other hand, for recoil on events, both total momentum conservation and track p_{T} bins qualitatively agree exceptionally well with the data from the CMS collaboration in Figure 4.7 [1]. The soft p_{T} recoil tracks dominantly contribute to the projected momentum outside cones about the leading jet axis, which improves upon previous MC results from a PYTHIA+HYDJET model to more closely resemble the data in Figure 4.9. This suggests that the recoil partons should be kept in the event and hadronized.

Still, the net momentum of the average recoil on event is non-zero, the remaining momentum imbalance being accounted for by the net momentum of the initial scattering centers. Evidently, the medium partons are sampled from a thermal distribution that is centered around zero, but has non-zero width. This remaining momentum of approx. $0 < p_{\mathrm{T}} < 50\mathrm{GeV}/c$ is likely to have an effect on the R_{AA} measured.

Another important limitation is that the recoiling partons do not undergo further rescattering. Therefore, after hadronization, the distribution of momenta of recoil hadrons is likely too hard, in comparison to the jets which may have undergone further quenching. Medium partons that do not scatter with the jet but instead interact softly with each other are not modeled. Hence, the observables presented for recoil on events improve upon those of recoil off events, but are still limited in their ability to validate experimental data.

One of the principal unresolved issues presented in [3] is that the disagreement between JEWEL excluding recoil partons and experimental data grows for increasing jet radii, as shown in Figure 4.5. The independence of jet R_{AA} on the cone radius used expands upon this disagreement. Conversely, for recoil on events, we find in Figure 4.21 a dependence of R_{AA} on the jet radius used. However, several obstacles prevent a direct comparison of these results to experimental data.

In particular, the validity of the background subtraction procedure is not certain. In general, the procedure used is not well suited for Monte Carlo events. The necessity for a background subtraction stems from the fact that including recoiling hadrons vastly increases the number of tracks in the event, as compared to the p+p benchmark events. In performing the subtraction, we have made the assumption that the recoil hadrons represent a background of soft p_{T} tracks that is independent from the rest

of the event. However, the recoil background in JEWEL is actually not independent from the high p_T parton that produced it, due to color connections between the partons as a result of the scattering. It is unknown what the exact effect and extent these connections will have on hadronization, particularly on the momentum distributions of the jet hadrons; however, it is highly likely that a correlation exists.

The distribution of recoil tracks in η is a peculiar feature of the model. Not only are recoil tracks dominantly generated about $\eta = 0$, but also independently of the high p_T parton showers that produced them. This is contrary to the expectation that recoil partons are co-moving with the jet, and suggests that JEWEL generates the recoil tracks at an η that may not be physically correlated with the jets.

Hence, we proposed strip regions constant in η to sample the background density from, leading to background densities ρ that are independent of the jet from which the background is being subtracted. This presents a contradiction in that jets in regions of low activity share the same background density as jets in regions of high activity. However, the analysis follows experimental cutoffs in [7] taking jets with $|\eta| < 0.5$ when calculating R_{AA}. Due to the low variation in jet p_T/A seen in this region in Figure 4.16, the strip regions of constant width can be taken as a simple approximation of the background density.

Furthermore, the recoil tracks distribution in η opposes the theory that recoil partons are expected to be co-moving with the parton shower and hence generated about the jet. Therefore, it is unclear whether the location of a recoil track in η is correlated with the location of the jet in η. This also pose the question of whether the observed trend in R_{AA} with increasing jet radius is a physically valid tendency. The cross section plots presented in Section 4.3 follow the tendency that jets will increase in momentum with increasing jet radius, since it is expected that a larger radius recovers more of the recoil track momenta. However, the width of the distribution of recoil tracks in η is finite at approx. $|\eta| < 2$. Hence, for a jet radius beyond $R \approx 1.0$, no further momentum is recovered. Furthermore, the shapes of the distributions in Figure 4.16 is not uniform, falling off from a peak at $\eta = 0$ to zero at $|\eta| \approx 2$. Hence, inside this strip region, the amount of momentum recovered does not scale only with the area of the jet, but instead also falls off based on the location of the jet in η.

For the R_{AA} measurements, a cutoff in jet $|\eta| < 0.5$ was used, following experiment in [7]. In this region, jet p_T/A is relatively constant; however, we see that from the projections in Figure 4.16 that it both falls off with increasing $|\eta|$ and varies slightly with jet radius. While a radius independent ρ value was proved to be a good first approximation, the non-constant background in η may hint that there may exist a more optimal, radius dependent trend in ρ.

The background subtraction also introduces a new variable to the analysis. Results from both experimental and MC models for jet quenching observables depend strongly on the jet reconstruction parameters, particularly the cone radius and algorithm used. Introducing the background subtraction to the MC model was shown to again produce results that are highly dependent on the region sampled for the background density.

6 Conclusions

In this thesis the hard probe observables of jet quenching in JEWEL were calculated. By default, JEWEL solely models the interactions of the jet with the medium. We focused on the role that including recoil tracks from the interaction with the medium ("recoil flag on" events) has on jet quenching observables as compared to excluding them ("recoil flag off") events.

First, the results presented in [3] [4] for the model were verified. The event asymmetry distributions for recoil flag on, off, and vacuum events were in good qualitative agreement with both experimental and previous MC data. For recoil flag off events, measurements of the nuclear modification factor R_{AA} for jet and charged hadron spectra both matched previous results. However, the reconstruction of jets using algorithms with a cone radius parameter R is clearly expected to affect the suppression measured. Increasing the cone radius is expected to yield fewer jets of higher p_{T}, shifting the R_{AA} toward unity. The failure to see this effect in JEWEL events where recoil hadrons are excluded begs a closer examination of these hadrons.

Momentum conservation in the model was verified to examine why momentum was not recovered with increasing jet radius. Momentum is conserved at each vertex in JEWEL. However, the scattering centers that compose the medium are generated with non-zero net momentum. Even when recoil hadrons are included, this momentum is carried by the final state particles.

Similar to in experimental data, the recoil particles represent a part of the underlying event that needs to be subtracted from the reconstructed momentum of the jet to study the true effect of jet quenching. While the recoil hadrons are not uncorrelated from the high p_{T} jets, we showed that it is possible to subtract an uncorrelated background of recoil tracks following the procedure in [13].

The recoil tracks are generated in strip in pseudorapidity of constant width $|\eta| < 2$, suggesting that the background density ρ should be independent of the jet finding radius R used. After testing several regions to sample ρ, it was shown that sampling from the region $S_{1.0} : |\eta| < 1.0$ yields the most radius R independent ρ values.

After performing the background subtraction from the reconstructed jets, the R_{AA} distributions as a function of jet p_{T} were measured for recoil flag on events for various jet radii. It was found that the nuclear modification factor increases at an approximately constant "rate" with increasing jet radius, although it is unclear at which cone radius it will reach unity, if at all. Furthermore, at low radii $R \leq 0.3$ a slight positive correlation of R_{AA} with increasing jet p_{T} was observed, as is also present in experimental data. This dependence was not observed at larger radii.

Several unresolved issues remain. In particular, the distribution of recoil particles in η raises the concern of whether theses tracks are physically realistic, or if their distribution is arbitrary if it has a negligible effect on observables. Assessing whether there exists a correlation between recoil particle p_{T} and hard scattered jet p_{T} may be of future interest, if the output of JEWEL can be modified.

In general, unbiased comparisons of R_{AA} to experimental data are difficult, as the entire event is not modeled by JEWEL, nor most MC models. The principal difficulty lies in model-

ing the soft interactions of the medium, which occur in a regime that cannot be described well by pQCD. Including recoil tracks and treating them as the underlying event lays out a foundation for the ultimate goal of modeling and analyzing the full event.

Acknowledgements

I want to thank my supervisors Marco van Leeuwen and Misha Veldhoen for their invaluable guidance, all the interesting and helpful discussions, and of course, the time they took to proof read my thesis. I would also like to thank my parents for the opportunity for me to come and study at the Subatomic Physics group in Utrecht, and for the wonderful time I spent there.

A Background Density σ Distributions

Region	Mean [GeV/c]	RMS [GeV/c]
S_{2R}	2.696	1.320
$S_{0.5}$	1.793	1.100
$S_{1.0}$	1.588	0.901
$S_{2.0}$	2.098	0.953

Table A.1: Mean and RMS values of the σ distributions in Figure 4.17, for the four regions sampled for the background density ρ in Section 4.3.

References

[1] C. Collaboration, (2011), 1102.1957v2, Phys.Rev.C84:024906,2011.

[2] D. d'Enterria, (2009), 0902.2011v2.

[3] K. C. Zapp, F. Krauss, and U. A. Wiedemann, (2012), 1212.1599v1.

[4] K. Zapp, G. Ingelman, J. Rathsman, J. Stachel, and U. A. Wiedemann, (2008), 0804.3568v2, Eur.Phys.J.C60:617-632,2009.

[5] B. Alver *et al.*, Phys.Rev. **C77**, 014906 (2008), 0711.3724.

[6] K. Nakamura and P. D. Group, Journal of Physics G: Nuclear and Particle Physics **37**, 075021 (2010).

[7] M. Verweij and for the ALICE collaboration, (2012), 1208.6169v2.

[8] M. Cacciari, G. P. Salam, and G. Soyez, (2011), 1111.6097v1.

[9] M. Cacciari, G. P. Salam, and G. Soyez, (2008), 0802.1189v2, JHEP 0804:063,2008.

[10] M. Gyulassy and X.-N. Wang, Comput.Phys.Commun. **83**, 307 (1994), nucl-th/9502021.

[11] N. Armesto, L. Cunqueiro, and C. A. Salgado, (2008), 0809.4433v1, Eur.Phys.J.C61:775-778,2009.

[12] T. Sjostrand, S. Mrenna, and P. Z. Skands, JHEP **0605**, 026 (2006), hep-ph/0603175.

[13] M. Cacciari, J. Rojo, G. P. Salam, and G. Soyez, (2010), 1010.1759v1, Eur.Phys.J.C71:1539,2011.

[14] CMS Collaboration, V. Khachatryan *et al.*, Phys.Rev.Lett. **105**, 022002 (2010), 1005.3299.